

Egyptian Journal of Chemistry

http://ejchem.journals.ekb.eg/



Electrochemical and Supercapacitive Properties of 4-((2-(5-((4-nitrophenyl)azo)-4-phenylthiazol-2-yl)hydrazineylidene)methyl)-benzoic acid (NTBA): Modified Electrodes for Sensing and Biomedical Applications



Ahmed M. Sarhan^{1*}, Ehab Abdel-Latif¹, Esam A. Gomaa¹, Farid E. El-Dossiky², Amr M. Abdelghany^{3,4}, Safa A. Badawy¹

¹Chemistry Department, Faculty of Science, Mansoura University, 35516 Mansoura, Egypt.

²Chemistry Department, Faculty of Science, Port Said University, Egypt.

³Spectroscopy Department, Physics Research Institute, National Research Centre, 33 ElBehouth St., Dokki, 12311, Giza, Egypt

⁴ Basic Science Department, Horus university, International Coastal Road, New Damietta, Egypt

Abstract

A novel thiazole derivative, 4-((2-(5-((4-nitrophenyl)azo)-4-phenylthiazol-2-yl)hydrazineylidene)methyl)-benzoic acid (NTBA), was synthesized with an 89% yield and characterized using IR, UV-Vis, ¹H NMR, and ¹³C NMR spectroscopy. The compound exhibited a highly conjugated structure, as confirmed by spectroscopic analyses. Electrochemical studies revealed that NTBA-modified indium tin oxide (ITO) electrodes, enhanced with carboxymethyl cellulose (CMC), demonstrated superior supercapacitive performance, with a specific capacitance of 0.0916 F/g, significantly higher than that of conventional glassy carbon electrodes (0.05295 F/g). Cyclic voltammetry indicated selective interactions with Cu²⁺, Mn²⁺, and MnO₄ ¹ ions, following diffusion-controlled mechanisms. Antioxidant assays (DPPH and ABTS) showed NTBA's potent radical scavenging activity, with IC₅ ₀ values of 29.26 mg/L and 36.94 mg/L, respectively, highlighting its potential for biomedical applications. Molecular docking studies using the Molecular Operating Environment (MOE) software identified two binding poses of NTBA with the viral protein 7JWY (SARS-CoV-2 target), exhibiting free binding energies of -5.33 kcal/mol and -5.23 kcal/mol. Key interactions involved residues Lys129, Asn125, Val171 (Pose 1) and Lys529, Asn331, Gln580, Arg328 (Pose 2), suggesting potential antiviral properties. This study underscores NTBA's multifunctionality as a promising material for energy storage, environmental sensing, and biomedical applications, bridging advancements in electrochemistry, supercapacitor technology, and therapeutic research.

Keywords: Thiazole sensitizer; Cyclic Voltammetry; Super capacity; Antioxidant, COVID -19

1. Introduction

The co-sensitized DSSC utilizing MRS-4 alongside N719 demonstrated superior performance with 8.13% PCE versus 7.50% for N719 alone, featuring enhanced JSC and FF values despite slightly reduced VOC, while TD-DFT theoretical studies confirmed experimental findings, establishing MRS-1-4 co-sensitizers as promising candidates for advanced photovoltaic applications and providing crucial design insights for future DSSC optimization [1]. Thiazolo[5,4-d]thiazole-based D- π -A organic dyes that have been synthesized and characterized have bispentylpropylenedioxythiophene (ProDOT) moieties that provide broad, intense absorption of visible light. These dyes have impressive efficiencies of up to 7.71% in small-scale thin-layer DSSCs and 6.35% in larger transparent cells without coadsorbents. They also have exceptional thermal stability over 1000 hours at 85°C, which makes them ideal candidates for building-integrated photovoltaic applications [2].

Cyclic voltammetry of bulk/nano $CdCl_2$ with/without Ceftazidime assessed metal-ligand complexation, yielding solvation and kinetic parameters under varied conditions. Studies determined stability constants and thermodynamic values for Ceftazidime-cadmium interactions, supported by DFT calculations of the ligand and complex and examination of Sr^{2+} and Ca^{2+} chlorides in KNO₃ solution utilized a novel palladium electrode displaying inherent redox waves suitable for analytical quantification [3-5].

Cyclic voltammetry was successfully employed for the first time for the simultaneous detection of calcium in water containing humic acid (HA) and copper (II) ions. The significant separation in oxidation potentials between the metals (copper appearing as low-field doublet peaks versus calcium's high-field signal) enabled reliable quantification of both

*Corresponding author e-mail: ahmedmosbah7701@gmail.com; (Dr. Ahmed Sarhan).
Received Date: 04 May 2025, Revised Date: 13 June 2025, Accepted Date: 26 August 2025
DOI: 10.21608/EJCHEM.2025.381843.11708
©2026 National Information and Documentation Center (NIDOC)

elements. Detection limits were established at 6.91×10^{-4} mol/L for calcium in copper-free solutions and 2.89×10^{-3} mol/L in copper-containing HA solutions, while copper's detection limit reached 2.56×10^{-3} mol/L. This electrochemical approach demonstrates potential application for monitoring these physiologically essential yet potentially harmful metals in drinking water, beverages, and dairy products with high reliability [6].

Ion-exchange calcium electrodes enable direct measurement of ionized calcium in biological fluids. Serum [Ca⁺⁺] typically ranges from 0.94-1.33 mmol/L (mean 1.14 mmol/L) with minimal individual variation (~6%) over months. [Ca++] varies inversely with pH in serum and blood. Heparinized blood shows lower [Ca⁺⁺] than serum due to calcium-heparin complex formation. Neither total calcium nor ultrafiltrable calcium reliably indicates serum [Ca++]. About 81% of protein-bound calcium associates with albumin and 19% with globulins. While these electrodes permit novel investigations, they have limitations; high cost, membrane replacement needs, lack of temperature control, logarithmic response sensitivity, CO₂ loss issues, and potential cation interference. Sodium tungstate was examined using cyclic voltammetry with glassy carbon electrodes in acidic and neutral media. The cathodic reaction involves tungstate ion transfer to WO₂, while oxidation converts WO₂ to WO₃. Interaction with Congo red dye showed higher stability constants and more favorable Gibbs free energies in NaClO₄ than in HCl, with lower kinetic and solvation parameters in 0.1M NaClO₄. Cyclic voltammetry compared bulk and nano manganese sulfate using 0.1M KCl electrolyte and glassy carbon electrodes. Redox behavior was analyzed with and without Doxorubicin using a three-electrode system. Various scan rates were tested, and stability constants for manganese-Doxorubicin interactions were determined [7-10]. Gold electrode-based voltametric technique for strontium ion quantification, demonstrating linear concentration dependence and altered electrochemical behavior in rosemary extract presence. The extract demonstrates significant antibacterial effects against diverse microorganisms, while molecular docking analysis of its active compounds carnosol and carnosic acid reveals promising binding affinity to COVID-19 targets [11].

The creation of a thiazole-based molecule (NTBA) by our research represents an important step in material science since it possesses three distinct functional qualities in a single molecular structure: electrochemical activity, super capacitive behavior, and antioxidant capabilities. In order to integrate NTBA with ITO substrates and improve capacitance performance, we developed a novel electrode modification technique utilizing carboxymethyl cellulose. The paper provides the first thorough analysis of the interactions between NTBA and several metals ions (Cu²⁺, Mn²⁺) and MnO₄ ion, exposing extensive diffusion-controlled mechanisms. This material is a major improvement over traditional single-purpose materials because of its unique ability to work in both biological and electronic applications. Our multipurpose compound significantly advances the development of adaptable smart materials with cross-disciplinary usage by opening up new possibilities for energy storage devices, biomedical applications, and environmental sensing.

2. Experimental

2.1. Materials and methods

The chemicals CuCl₂·2H₂O, 4-((2-carbamothioylhydrazineylidene)methyl)benzoic acid, *N*-(4-nitrophenyl)-2-oxo-2-phenylacetohydrazonoyl bromide, dioxane and triethylamine (TEA) used are provided from Sigma-Aldrich Co. and used without purification. Deionized water was used. The aqueous solutions were prepared using distilled water. Before taking the measurement, all solutions were aerated with nitrogen gas for fifteen minutes using nitrogen gas free of oxygen. The standard three-electrode setup was employed. Measurements using cyclic voltammetry were performed using the DY2000 (USA) as the working electrode. The electrode served as the counter electrode and the Ag/AgCl electrode as the reference electrode [7-14].

2.2. General procedure for synthesis of sensitizer (NTBA):

In a 100 mL round-bottom flask, a mixture of 4-((2-carbamothioylhydrazineylidene) methyl) benzoic acid (1) (2.23 g, 0.01 mol) and N-(4-nitrophenyl)-2-oxo-2-phenylacetohydrazonoyl bromide (2) (3.50 g, 0.01 mol) in 40 mL of dioxane with drops of triethylamine (TEA) was refluxed. The reaction mixture was heated under reflux for 7 hours. The resulting red solid sensitizer was then filtered and washed with ethanol, yielding compound **NTBA**.

4-((2-(5-((4-Nitrophenyl) azo)-4-phenylthiazol-2-yl) hydrazineylidene) methyl) benzoic acid (NTBA):

Yield = 89%. M.p. Above 300 °C. IR (KBr) v_{max} . cm⁻¹: 3201 (N-H), 1715 (C=O), 1590 (C=N). UV/Visible spectral data was collected within the spectral range 200-1200 nm with spectral resolution 1nm. 1H NMR (DMSO- d_6 , ppm): δ 7.43 (d, J= 9.00 Hz, 2H, Ar-H), 7.61 (t, J= 7.00 Hz, 2H, Ar-H), 7.66 (t, J= 7.00 Hz, 1H, Ar-H), 7.98 (d, J= 8.50 Hz, 2H, Ar-H), 8.06 (d, J= 9.00 Hz, 2H, Ar-H), 8.21 (d, J= 9.00 Hz, 2H, Ar-H), 8.27 (d, J= 7.50 Hz, 2H, Ar-H), 8.74 (s, 1H, N=CH), 11.42 (s, 1H, N-H), 13.19 (s, 1H, COOH). ¹³C NMR (DMSO- d_6 , ppm): δ 125.5 (2C), 127.8 (2C), 128.4 (3C), 129.8 (2C), 130.5 (3C), 135.9, 141.2, 144.5, 146.7, 148.8, 151.5, 155.5, 159.5, 162.7, 166.8, 172.6. Analysis Calcd. for C₂₃H₁₆N₆O₄S (472.48): Calculated: C, 58.47; H, 3.41; N, 17.79 %. Found: C, 58.57; H, 3.38; N, 17.87%.

2.3. Radical scavenging assay or antioxidant activity

The antioxidant efficiency from 4-((2-(5-((4-nitrophenyl)azo)-4-phenylthiazol-2-yl)hydrazineylidene)methyl)-benzoic acid was investigated by assessing their capacity to scavenge DPPH (2,2-Diphenyl-1-picrylhydrazyl) radicals [15]. The quantities of 5, 10, 20, 30, 40, and 50 mg L⁻¹ of 4-((2-(5-((4-nitrophenyl)azo)-4-phenylthiazol-2-yl)hydrazineylidene)methyl)-benzoic acid were obtained by diluting methanol. Rapidly mixing equal parts of freshly made 0.3 mM DPPH with each amount of the EO for 30 minutes at 25°C produced a reaction mixture. After that, a spectrophotometer (Analytik Jena, Jena, Germany) was used in order to analyze the absorbance at a wavelength of 517 nm. Ascorbic acid was administered to a control group using the same protocol at dosages of 1.0, 2.5, 5, 10, 15, and 20 mg L⁻¹. The DPPH radical scavenging activity (%) was estimated by the following equation:

DPPH radical scavenging (%) = $[(A control - A sample)/A control] \times 100$

The antioxidant capacity of 4-(2-(5-(4-nitrophenyl) diazenyl)-4-phenylthiazol-2-yl)-hydrazineylidene) methyl) benzoic acid was evaluated through its ability to neutralize ABTS radicals [16]. The compound was tested across concentrations ranging from 5-50 mg mL⁻¹. The experimental protocol involved combining 2 mL of freshly prepared ABTS solution with 0.2 mL of the synthesized thiazole derivative, followed by a 6-minute dark incubation period. Absorbance measurements at 735 nm were performed using an Electronic 22D spectrophotometer (Milton Roy, CA, USA). Ascorbic acid served as a reference standard. The ABTS radical scavenging capacity was calculated using the same inhibition percentage formula employed in the DPPH assay, where the difference between control and sample absorbance values was normalized to the control absorbance. This comprehensive radical scavenging assessment reveals the compound's distinctive multifunctional nature, representing a significant advancement in developing materials that simultaneously offer electrochemical sensing capabilities, supercapacitive properties, and substantial antioxidant activity, a combination rarely achieved in previously reported compounds.

2.4. Molecular docking

The Molecular Operating Environment (MOE) software version 2015.10 (Chemical Computing Group Inc., Montreal, Canada) conducted molecular docking between synthesized compounds and viral protein target (PDB ID: 7JWY). The researchers used Molecular Operating Environment (MOE) software to analyze how the synthesized compounds interacted with viral protein target PDB ID: 7JWY. Researchers extracted the protein structure from the RCSB Protein Data Bank before deleting water molecules and co-crystallized ligands and heteroatoms to avoid docking calculation errors. The Protonate 3D algorithm was used to add hydrogen atoms at physiological pH (7.4) followed by energy minimization with the AMBER12:EHT force field achieving gradient convergence of 0.1 kcal/mol/Å, the ligand structures were created using the ChemDraw 15 program [17,18].

3. Results and Discussion

3.1. Synthesis of thiazole-based sensitizer (NTBA)

In the first step, hydrazonoyl bromide (1) is prepared by combining phenacyl bromide with the diazonium salt of 4-nitroaniline in ethanol solution and sodium acetate, resulting in the formation of N-(4-nitrophenyl)-2-oxo-2-phenylacetohydrazonoyl bromide, following established methods [19]. In the second step, thiosemicarbazone derivative (2) was synthesized by reacting thiosemicarbazide with p-carboxylbenzaldehyde in the presence of ethanol and a few drops of acetic acid, yielding 4-((2-carbamothioylhydrazineylidene) methyl) benzoic acid (2), as previously reported in the literature [20]. In the final step, the sensitizer (NTBA) was produced by reacting 4-((2-carbamothioylhydrazineylidene) methyl) benzoic acid (1) with N-(4-nitrophenyl)-2-oxo-2-phenylacetohydrazonoyl bromide (2) in dioxane and triethylamine under reflux for 7 hours. This reaction resulted in the formation of thiazole derivatives, as illustrated in Scheme 1. Various spectrum approaches and elemental studies were used to confirm the structure of the isolated thiazole sensitizer (NTBA). For example, peaks at 3201, 1715 and 1590 cm⁻¹ in the IR spectrum of sensitizer NTBA indicated the presence of NH, C=O and C=N groups, respectively Fig. 1. The ¹H NMR spectrum displayed two singlet signals δ 11.42 and δ 13.19 ppm, corresponding to the amino (N-H) and carboxylic (COOH) groups. Fourteen aromatic protons were observed between δ 7.43 and δ 8.27 ppm. At δ 8.74 ppm, a singlet indicating the presence of a CH=N proton was discovered Fig. 2. The ¹³C NMR spectrum showed a prominent signal at δ 166.9 ppm, corresponding to the carbonyl in the carboxylic group (COOH). Fig. 3

Scheme 1. Synthesis of thiazole sensitizer NTBA.

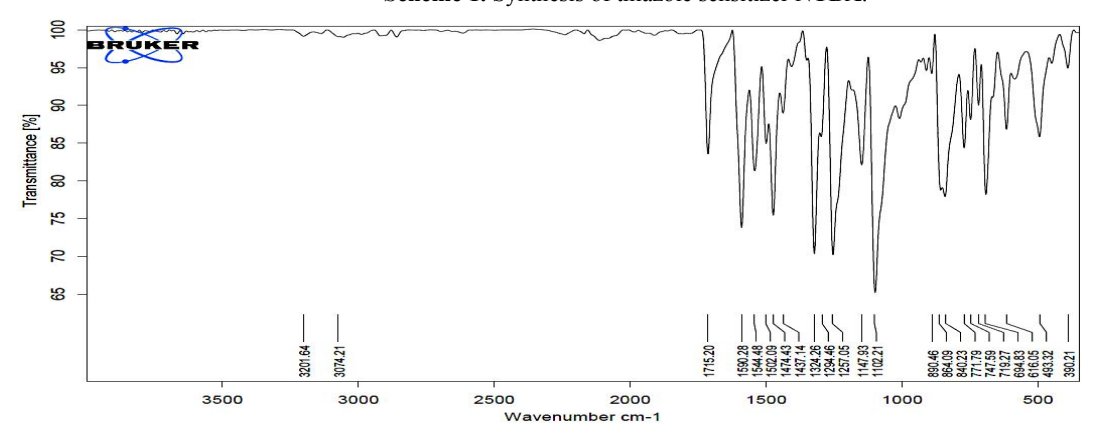


Fig. 1. IR spectrum of sensitizer NTBA.

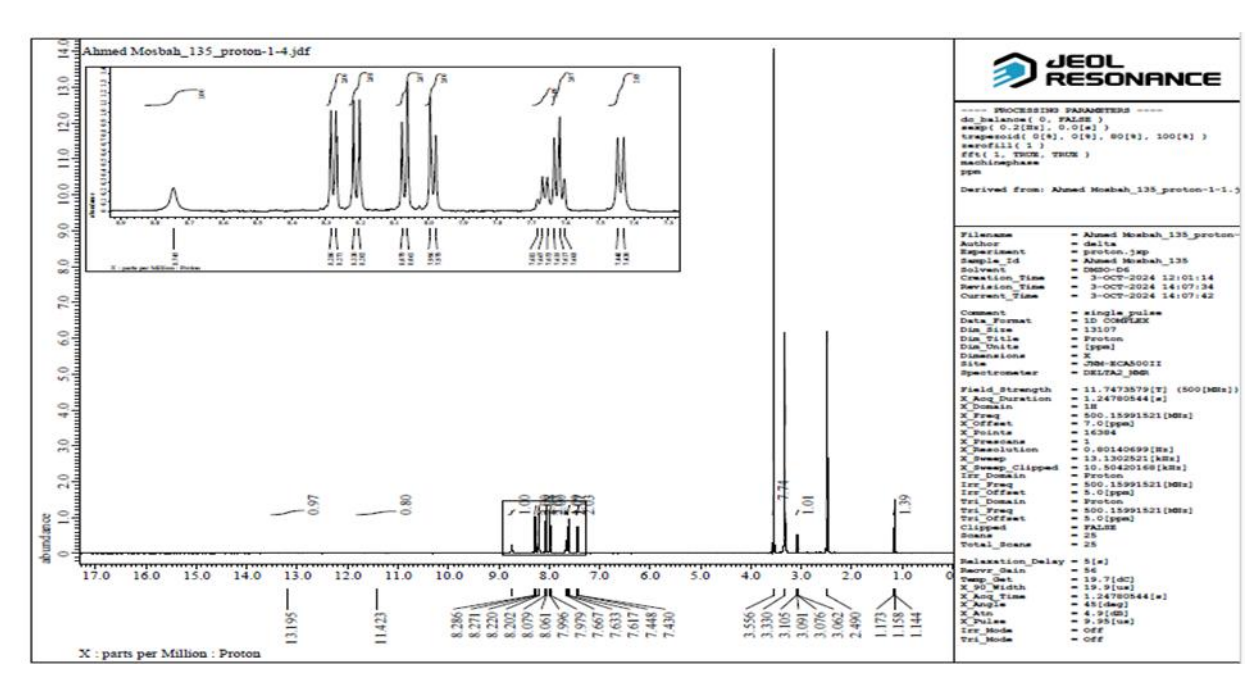


Fig. 2. ¹H NMR spectrum of sensitizer NTBA.

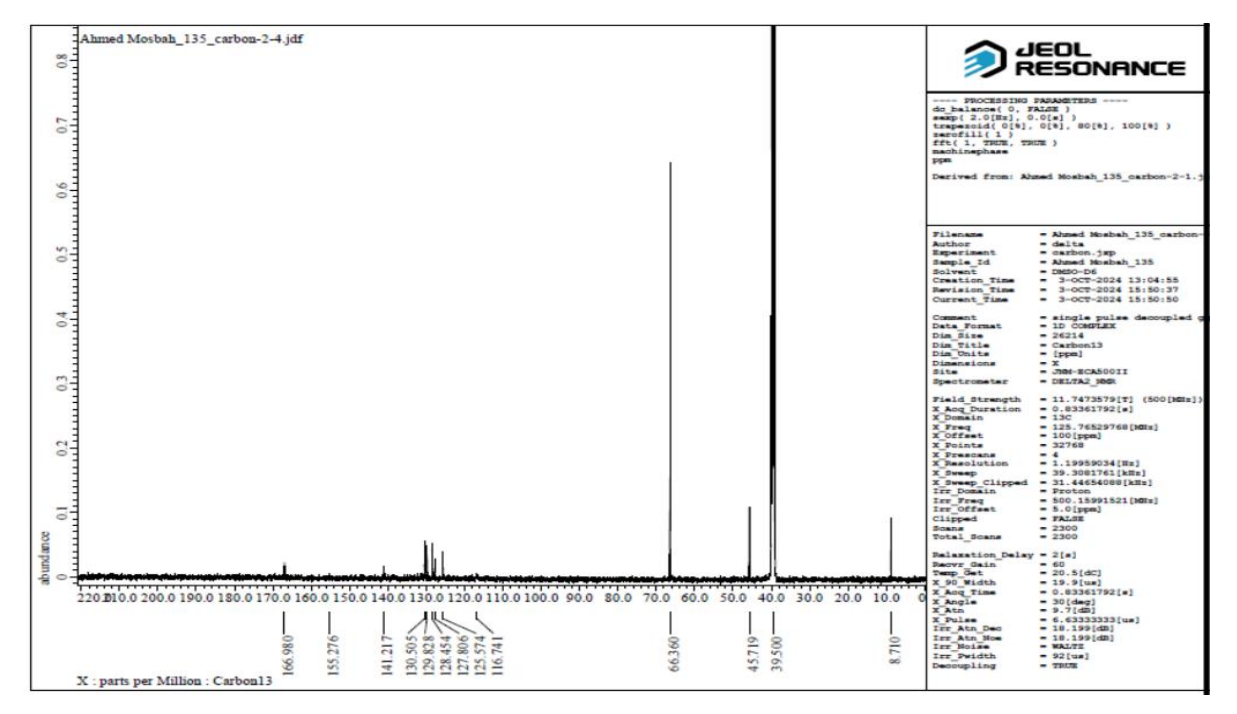


Fig. 3. ¹³C NMR spectrum of sensitizer NTBA

3.2 Photophysical properties

The UV-Vis absorption spectrum reveals three distinct peaks providing insights into the compound's electronic structure. The spectrum exhibits a weak absorption band at 898 nm, likely representing an n- π^* transition, though its negative value suggests it might be baseline noise. The most prominent peak appears at 528 nm with a high absorption coefficient, indicating a strong π - π^* transition arising from the extensive conjugation in the molecule's structure. Additionally, a moderately intense peak at 264 nm corresponds to another π - π^* transition at higher energy, typically associated with localized conjugated segments. The presence of both n- π^* and π - π^* transitions, combined with the varying intensities and wavelengths, confirms the molecule's well-conjugated system with potential heteroatoms, enabling multiple electronic transitions through extended π -electron delocalization. Fig. 4

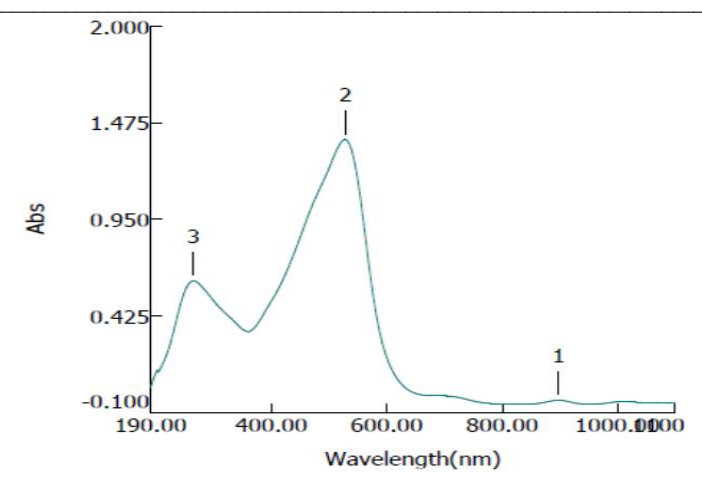


Fig. 4. UV-Vis spectra of NTBA recorded in DMF (2 $\times 10^{-5}$ M)

The molecular computation study of NTBA demonstrates key electronic features through its planar framework and extended π -conjugation system. Analysis of the MEP mapping highlights polarized charge distribution, with electron density concentrated in conjugated segments and depleted zones near electron-withdrawing functionalities. The frontier molecular orbital calculations reveal balanced electron distribution in the HOMO state and effective spatial separation in the LUMO configuration, supporting strong charge-transfer capabilities. These computational insights, combined with the optimized structural characteristics, indicate NTBA's significant potential for implementation in charge transport and photon-harvesting electronic devices. Fig. 5

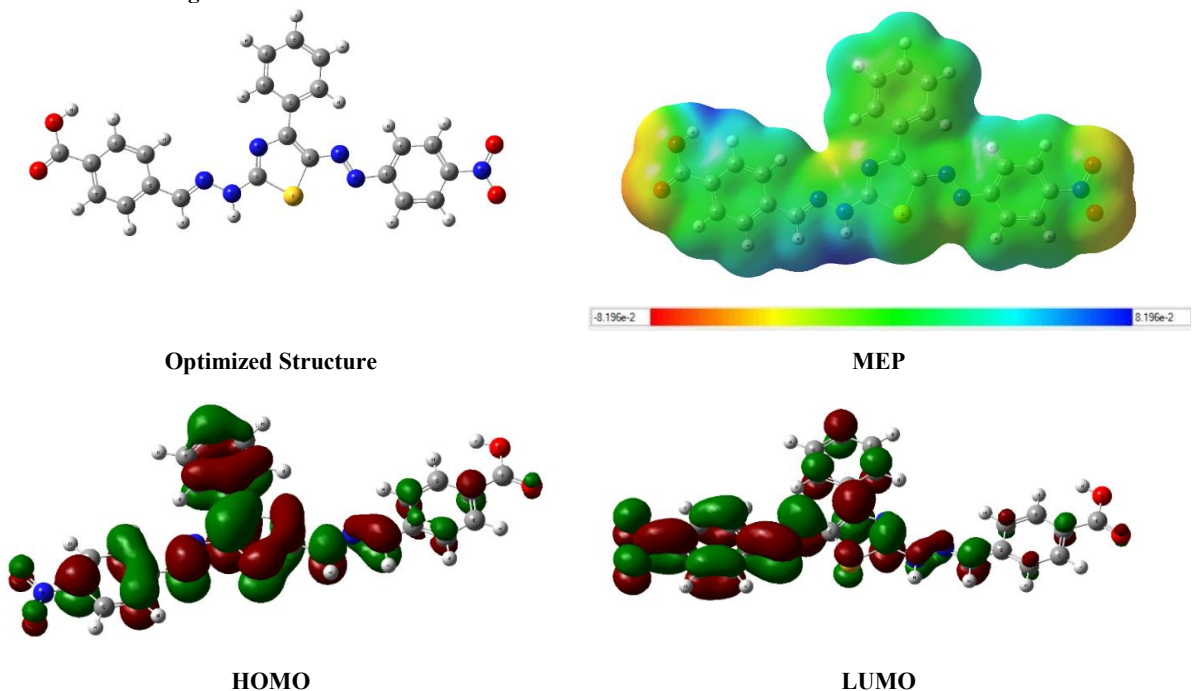


Fig. 5. Optimized electron distribution and MEP for compound NTBA.

3.3. Electric Super capacity studies for 4-((2-(5-((4-nitrophenyl)azo)-4-phenylthiazol-2-yl)hydrazineylidene)methyl)benzoic acid (NTBA).

Polymer binders are essential for improving electrode-substrate interfacial characteristics for improved electrochemical performance, which is why adding 1 mL of 0.5% carboxymethyl cellulose (CMC) binder to the ITO substrate resulted in a considerable improvement in the electrode's electric capacity. Because it forms good films, is water soluble, and exhibits strong electrical stability, CMC is a conventional choice for energy storage solutions. However, researchers need to come up with new technical methods that go beyond what is currently known in scientific literature. Since low concentrations improve ion transport without sacrificing mechanical strength and high concentrations improve adhesion but reduce active site, research should concentrate on determining the optimal binding efficiency level by methodically testing CMC concentrations between 0.1% and 2.0% to minimize inactive material content while achieving optimal performance targets. The creation of

advanced composite binders by mixing CMC with conductive polymers allows for the simultaneous supply of mechanical support and enhanced electron mobility to offset the inherent insulating qualities of CMC.

The strategic direction requires a new focus on demonstrating exceptional performance characteristics using extensive electrochemical analysis methods that include multiple scan rates in cyclic voltammetry to measure better charge storage properties as well as improved capacitive response and galvanostatic charge-discharge tests to assess how well the device maintains its capacity under high current conditions while measuring ion transport speeds and impedance spectroscopy that identifies resistance levels and diffusion rates along with interfacial characteristics before and after extended cycling periods. The comparative analysis between traditional electrodes and new designs needs to focus on two key areas that demonstrate better electrode performance: measurable specific capacitance enhancements and long-term cycling stability improvements across thousands of charge-discharge cycles which reveal enhanced mechanical and electrochemical resistance and improved ability to maintain excellent power density for advanced energy storage applications.. Fig. 6.

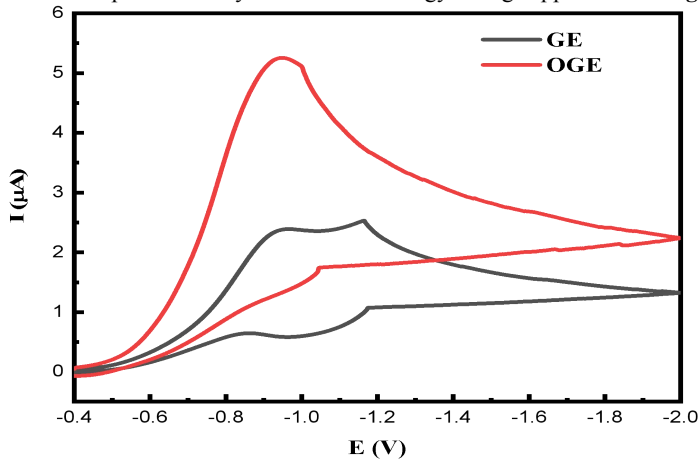


Fig. 6. Cyclic voltammograms of solid Glass E & NTBA Electrode in 0.1 M NaOH at 296.15 K

Capacitors use two conductive plates that are isolated from one another by an insulator to store electrical charge. On each plate, opposing charges build up when voltage is applied. Plate area, insulator characteristics, and plate separation all affect capacitance; smaller separations (not bigger) result in higher capacitance.

With far higher energy and power densities than traditional capacitors and batteries, supercapacitors—also known as ultracapacitors or EDLCs—represent cutting-edge capacitor technology. Their remarkable cycle life, high power density, fast charge-discharge capabilities, and capacitance values of hundreds of farads are some of their main advantages. Supercapacitors are useful for energy storage and power regulation applications because, in contrast to conventional capacitors, they store energy electrostatically at the electrode-electrolyte interface The established electrode, which uses carboxymethyl cellulose on ITO, should highlight any new structural arrangements, material combinations, or interface features that provide quantifiable performance gains over previous supercapacitor designs. The electric double layer capacity in F/gram was calculated following the given equation with item identification. The electric capacity of the prepared new electrode is very large in comparison to the standard glassy carbon electrode Table 1.

The scan rate effect, which results the greater voltammograms than others, indicates the plausibility of the new material electrode as a good working electrode and a supercapacitor material. A new material electrode shows potential to function as a suitable working electrode and supercapacitor material according to the increased voltammograms created by the scan rate effect. The Glass E and 4-((2-(5-((4-nitrophenyl) azo)-4-phenylthiazol-2-yl) hydrazineylidene) methyl) benzoic acid (NTBA) composite electrode charge storage mechanisms are revealed through systematic scan rate analysis between 0.01 and 0.1 V/s. **Fig. 7**

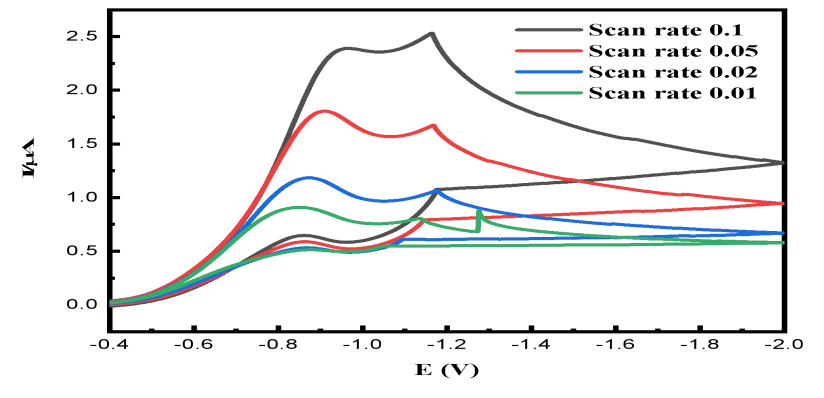


Fig. 7. Scan rates of Glass E and NTBA new electrode.

Table 1: Comparison of the area and electric capacity of the prepared new material electrode (NTBA).and Glassy carbon electrode (Glass E) in 0.1 M

Area (AV)	scan rate (v/s)	Mass (g)	potential window	Cp (F/g)		
mea (mv)	Scan rate (v/s)	1V1033 (g)	(v)			
2.14E-04	0.1	0.01	1.6	0.066804	(NTBA)	
1.16E-04	0.05	0.01	1.6	0.072298	(NTBA)	
7.51E-05	0.02	0.01	1.6	0.117371	(NTBA)	
3.53E-05	0.01	0.01	1.6	0.110298	(NTBA)	
1.07E-04	0.1	0.01	1.6	0.033388	Glass E	
7.22E-05	0.05	0.01	1.6	0.045108	Glass E	
3.84E-05	0.02	0.01	1.6	0.060003	Glass E	
2.35E-05	0.01	0.01	1.6	0.073308	Glass E	

Cp of (NTBA) = 0.0916 F/g

Cp of Glass E = 0.05295 F/g

$$Cp = \frac{A}{2mk(v_2 - v_1)}$$

Where m = mass of material (g), (v2-v1) = potential window (V), k = scan rate (v/s), A = area, and Cp = specific capacitance

$3.4. \ Cyclic \ voltammetry \ of \ MnCl_2 \ and \ KMnO_4 \ in \ 0.1 \ M \ NaOH \ using \ 4-((2-(5-((4-nitrophenyl)\ azo)-4-phenylthiazol-2-yl)\ hydrazineylidene) \ methyl) \ benzoic \ acid \ (NTBA) \ electrode \ deposited \ on \ ITO \ conducting \ glass \ at \ 296.15 \ K.$

The cyclic voltammetry was performed in 0.1 m NaOH using the new prepared working electrode of 4-((2-(5-((4-nitrophenyl) azo)-4-phenylthiazol-2-yl) hydrazineylidene) methyl) benzoic acid (NTBA) stacked in ITO nano glass slide. The solvation parameters for MnCl₂ evaluated following different equations [21-47] are given in **Table 2** with an increase in

all values by an increase in MnCl₂ concentration, proving a diffusion-controlled reaction. **Fig.8**

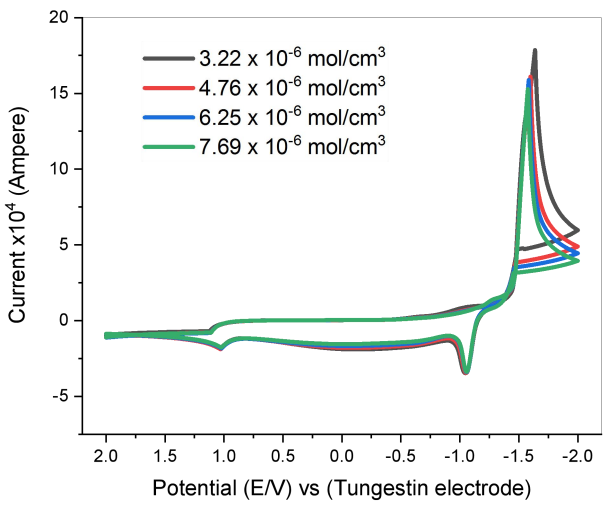


Fig. 8. Different concentrations of MnCl₂. In 0.1 M NaOH

Egypt. J. Chem. **69,** No. 2 (2026)

Table 2. Electrochemical solvation parameters of MnCl₂ using 4-((2-(5-((4-nitrophenyl) azo)-4-phenylthiazol-2-yl) hydrazineylidene) methyl) benzoic acid (NTBA) electrode deposited in ITO glass.

MnCl₂ at 296.15 K (scan rate 0.1) first peak

M x10 ⁻⁶	Ep,a (volt)	Ep,c (volt)	ΔEp (volt)	ipa	ipc	in / in
				x10 ⁻⁴ (Amp)	x10 ⁻³ (Amp)	ip _a / ip _c
3.22	-1.046	-1.635	0.589	3.325	1.380	0.241
4.76	-1.044	-1.600	0.556	3.156	1.257	0.251
6.25	-1.056	-1.582	0.525	3.551	1.256	0.283
7.69	-1.056	-1.575	0.519	3.326	1.207	0.276

		MnCl ₂ at 296.15 K (scan rate 0.1) first peak								
M	E°	Da	Dc			ks	Γ _c x10 ⁷	(+)	Га х10-8	(-)
x10 ⁻	(volt)	x10 ⁻⁵	x10 ⁻	Ep _{c/2}	αn _a	x10 ⁺⁵	(mol/cm ²)	Qcx10 ⁴	(mol/cm ²)	
3.22	-1.341	1.936	3.33	-1.706	0.701	-4.72	1.213	7.35	2.923	1.77
4.76	-1.322	8.002	1.27	-1.644	1.137	-1.17	1.105	6.70	2.775	1.68
6.25	-1.319	5.878	7.35	-1.623	1.190	-1.46	1.103	6.69	2.121	1.89
7.69	-1.315	3.404	4.48	-1.613	1.294	-1.23	1.061	6.43	2.924	1.77

On adding $KMnO_4$ to $MnCl_2$ the cathodic peak mentioned in Fig. 9. is shifted in potential towards a more negative one indicating interaction between the two materials, also the anodic peak is shifted to more positive potentials indicating the same trend as that for reduction.

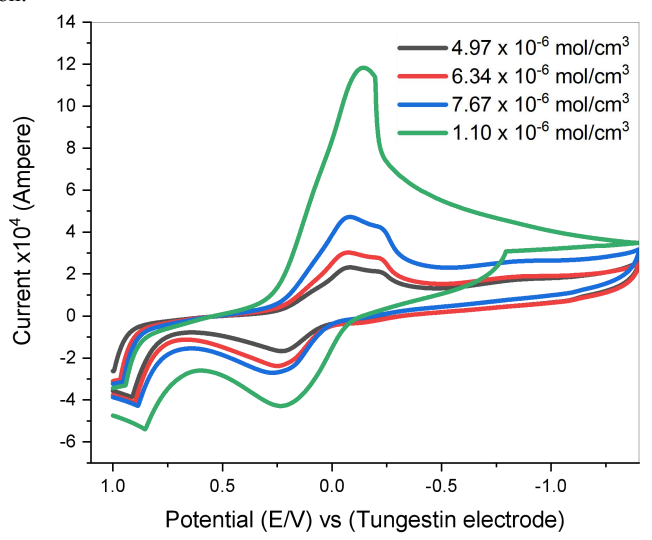


Fig. 9. Different KMnO₄ concentrations added to MnCl₂ using 4-((2-(5-((4-nitrophenyl) azo)-4-phenylthiazol-2-yl) hydrazineylidene) methyl) benzoic acid (NTBA) electrode versus tungsten auxiliary electrode.

3.5. Cyclic voltammetry data for redox reaction of CuCl₂ with 4-((2-(5-((4-nitrophenyl) azo)-4-phenylthiazol-2-yl) hydrazineylidene) methyl) benzoic acid (NTBA) in 0.1 M HNO₃ using glassy carbon electrode:

Different concentrations for $CuCl_2$ were used for cyclic voltammetry study **Table 3** in 0.1 M HNO₃ **Fig. 10** and also in the presence of different additions from ligand 4-((2-(5-((4-nitrophenyl) azo)-4-phenylthiazol-2-yl) hydrazineylidene) methyl) benzoic acid (NTBA) as given in **Fig. 11**.

Table 3 . Effect of different concentrations of $CuCl_2$ in 0.1 M HNO₃ by using a glassy carbon working electrode at a scan rate 0.1V/s and 295.75 K.

[M] x10 ⁻⁶		Volt		Aı	тр	In o/In o	Volt
mol.L ⁻¹	(-) Ep,a	Ep,c	$\Delta \mathbf{E} \mathbf{p}$	(-)Ip,ax10 ⁻⁴	Ip,cx10 ⁻⁴	Ip,a/Ip,c	E°
2.60	0.142	-0.1138	0.2563	9.63	3.31	2.908	0.0142
3.85	0.261	-0.2587	0.5201	1.25	8.19	1.529	0.0013
5.06	0.232	-0.2373	0.4702	2.28	1.56	1.465	-0.0022
6.25	0.237	-0.2347	0.4725	3.13	1.87	1.677	0.0015
7.41	0.227	-0.2116	0.4392	2.44	1.49	1.632	0.0080
7.98	0.215	-0.2288	0.4441	3.29	2.38	1.383	-0.0067

Dax 10 ⁵ cm ² .s ⁻¹	Dc x10 ⁻⁵ cm ² .s ⁻¹	Epc/2	Epa-Epc/2	α_{na}	k _{sc} x10 ² cm ² .s ⁻¹	Γc x10 ⁻⁹ mol.cm ⁻²	(+)Qcx10 ⁻⁵ Columb	Γax10 ⁻⁹ mol.cm ⁻²	(-)Qax10 ⁵ Columb
2.60	2.61	-0.0161	0.0977	0.4473	1.13	2.5721	1.56	7.4822	4.53
3.85	7.30	-0.1492	0.1095	0.3991	4.83	6.3626	3.86	9.7343	5.90
5.06	1.52	-0.1376	0.0996	0.4385	2.53	1.2108	7.34	1.7748	1.08
6.25	1.43	-0.1549	0.0797	0.5478	2.88	1.4495	8.78	2.4313	1.47
7.41	6.53	-0.1286	0.0829	0.5268	9.41	1.1593	7.02	1.8927	1.15
7.98	1.43	-0.1387	0.0901	0.4849	1.48	1.8483	1.12	2.5566	1.55

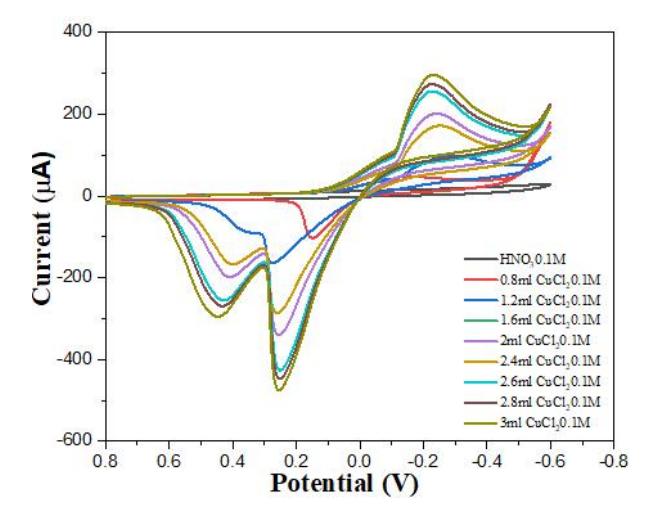
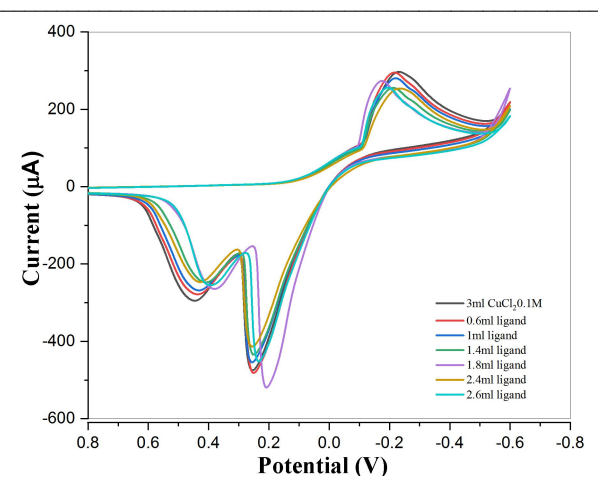


Fig. 10. Cyclic voltammogram of different concentration of CuCl₂ (0.1M) in 30 ml HNO₃ (0.1M) and scan rate 0.1V.s⁻¹



 $Fig.~11.~Cyclic~voltammogram~of~different~concentrations~of~ligand~in~CuCl_2~(0.1M)~in~30~ml~HNO_3~(0.1M)~and~scan~rate~0.1V.s^{-1}$

The scan rate effect, which is the greater voltammograms than others, indicates the plausibility of the new material electrode as a good working electrode and supercapacitor material. **Fig .12.** The analysis data following different equations as cited in references [19-42] are given in Tables 4 and 5.

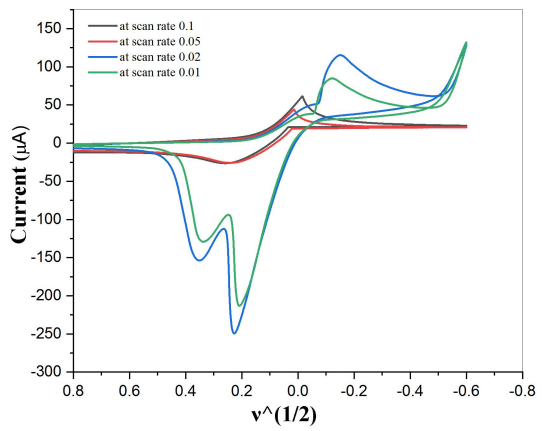


Fig. 12. Cyclic voltammogram of different scan rate of CuCl₂ and different concentration of ligand in 30 ml HNO₃ (0.1M) and scan rate 0.1V.s⁻¹

Table 4. Effect of different concentrations of HNO₃+CuCl₂ by using an electrode at different scan rates and 295.75 K.

Scanrate	Volt	Volt					volt
(v/sec)	(-)Ep,a	Ep,c	ΔΕρ	(-)Ip,ax10 ⁵	Ip,cx10 ⁻⁵	Ip,a/Ip,c	E°
0.1	0.2549	0.0184	0.23651	2.95	3.71	0.7939	0.1366
0.02	0.2184	0.0490	0.16933	2.99	2.50	1.1958	0.1337
0.01	0.2209	-0.1328	0.35379	2.45	9.97	2.4620	0.0440
0.005	0.1944	-0.1172	0.31170	1.88	7.69	2.4434	0.0386

scan rate (v/sec)	Epc/2	Epa-Epc/2	α_{na}	k _{sc} x10 ² cm ⁻² .s ⁻¹	Γc x10 ⁻²	9 (+)Qcx10 ⁵ coulomb	Γa x10 mol.cm ⁻²	9 (-)Qax10 ⁵ coulomb
0.1	0.07225	0.0538	0.8121	3.38	2.8844	1.75	2.28997	1.39
0.02	0.10922	0.0601	0.7266	5.17	9.7033	5.88	1.16036	7.03
0.01	-0.0835	0.04928	0.8868	1.15	7.74586	4.69	1.90705	1.16
0.005	-0.0621	0.05506	0.7937	3.42	1.19517	7.24	2.92036	1.77

An increase in most data was observed, indicating a diffusion-controlled reaction.

Table 5. Stability constant for (CuCl2+ligand) interaction

[L]x10 ⁻⁶	Metal	Complex	A.E	1 0:	$\Delta \mathbf{G}$
mol.L ⁻¹	(Ep,a)M	(Ep,a)C	ΔE mv	log βj	(kJ /mol)
8.93	0.0163	0.0161	0.00012	1.2032	-0.52066
8.82	0.0163	0.0157	0.000578	2.1015	-0.90940
8.72	0.0163	0.0089	0.007344	5.7906	-2.50574
8.62	0.0163	0.0218	-0.00557	0.6866	-0.2971
8.47	0.0163	0.0077	0.008522	7.93524	-3.43378

Small Gibbs free energies were obtained for the interaction of CuCl₂ with the prepared ligand, indicating small interaction.

3.6 Antioxidant activity

The study evaluated the antioxidant activity of 4-(2-(5-(4-nitrophenyl) diazenyl)-4-phenylthiazol-2-yl) -hydrazineylidene) methyl) benzoic acid (NTBA) using DPPH and ABTS radical scavenging assays, with ascorbic acid as a standard. (NTBA) Table 6 showed concentration-dependent antioxidant activity in both assays, with IC50 values of 29.26 mg/L for DPPH and 36.94 mg/L for ABTS. The highest scavenging activity for NTBA was observed at 50 mg/L, reaching 78.84% for DPPH and 63.52% for ABTS. Ascorbic acid demonstrated higher antioxidant potency, with lower IC50 values of 11.20 mg/L for DPPH and 12.49 mg/L for ABTS. Statistical analysis indicated significant differences between concentrations for both (NTBA) and ascorbic acid (LSD0.05). The results indicate that (NTBA) possesses notable antioxidant properties, albeit less potent than ascorbic acid. The concentration-dependent increase in radical scavenging activity suggests that (NTBA) contains compounds capable of neutralizing free radicals. The difference in IC50 values between DPPH and ABTS assays may be due to the varying mechanisms of these methods or the nature of antioxidants present in (NTBA). While (NTBA) shows promise as an antioxidant, further studies are needed to identify its active components and evaluate its potential for practical applications. The lower potency compared to ascorbic acid suggests that higher concentrations of (NTBA) may be required to achieve similar antioxidant effects in potential applications.

Table 6: DPPH and ABTS radicals scavenging activity percentage and the IC₅₀ values by sample and ascorbic acid as standard.

	G	Scavenging activity	(%)			
Treatment	Conc.	DPPH		ABTS		
	(mg/L)	RSA (%)	IC ₅₀ (mg/L)	RSA (%)	IC ₅₀ (mg/L)	
(NTBA)	5	13.4±0.74		12.047±0.67		
	10	21.74±1.21		17.21±0.96		
	20	34.59±1.92	20.26	28.677±1.59	26.04	
	30	56.38±3.13	29.26	43.15±2.40	36.94	
	40	64.82±3.60		55.86±3.10		
	50	78.84 ± 4.38	78.84±4.38			
	LSD _{0.05}	S4.02***				
Ascorbic acid	1	6.3±0.35		3.64±0.21		
	2.5	15.52±0.86		11.86±0.66		
	5	42.24±2.35	11 20	38.58 ± 2.14	12 40	
	10	54.78±3.04	11.20	47.12±2.62	12.49	
	15	61.07±3.39		57.41±3.19		
	20	74.22±4.12		70.56±3.92		
	LSD _{0.05}	9.76***				

3.7. Molecular docking

The docking results show two binding modes for 4-(2-(5-(4-nitrophenyl) diazenyl)-4-phenylthiazol-2-yl) -hydrazineylidene) methyl) benzoic acid (NTBA) with the viral protein, with free energy binding at -5.33 kcal/mol and -5.23 kcal/mol for Pose 1 and Pose 2, respectively. Pose 1 forms electrostatic and hydrophobic interactions with Lys129, Asn125, and Val171, while Pose 2 involves Lys529, Asn331, Gln580, and Arg328 to form a relatively wider interaction network. Having an energy difference of only 0.1 kcal/mol, these two conformations are equally probable and demonstrate the conformational flexibility

of NTBA and its ability to bind at two sites. This dual binding behaviour can be exploited for antiviral action by two distinct binding mechanisms and enhanced resistance to viral mutations. These binding energies are comparable to those of known antiviral molecules, which makes NTBA a promising therapeutic drug with greater mutation resistance than that of single-site inhibitors.

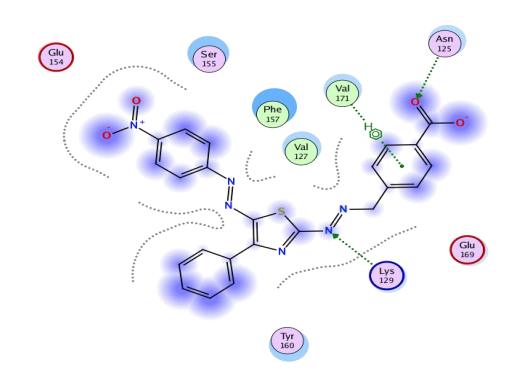
3.7.1 Binding Pose 1

634

Three major interactions with a combined energy contribution of -3.9 kcal/mol are revealed by the first binding pose Table 7: one pi-H interaction between the ligand's 6-membered ring and Val171 (3.84 Å, -0.7 kcal/mol) and two hydrogen bond acceptor interactions (N9-Lys129 at 3.51 Å, -2.2 kcal/mol and O25-Asn125 at 3.04 Å, -1.0 kcal/mol).Fig.13, Fig.14.

Table 7: Most Efficient Docking Results of the (NTBA) and 7JWY: VIRAL PROTEIN / 7JWY (Pose 1)

Ligand	Receptor	Interaction	Distance	E (kcal/mol)
N9 15	NZ LYS 129 (A)	H-acceptor	3.51	-2.2
O25 35	ND2 ASN 125 (A)	H-acceptor	3.04	-1.0
6-ring	CG2 VAL 171 (A)	pi-H	3.84	-0.7



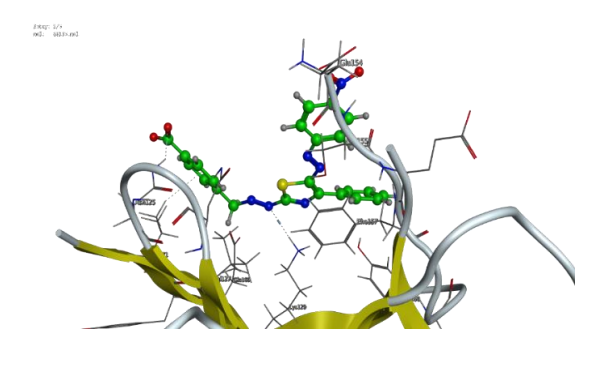


Fig. 13. 2D interaction between (NTBA) and VIRAL PROTEIN / 7JWY(Pose 1)

Fig. 14. 3D interaction between (NTBA) and VIRAL PROTEIN / 7JWY (Pose 1)

3.7.2 Binding Pose 2

Through the overall energy contribution of -14.5 kcal/mol, the second binding pose shows stronger interactions Table 8. These include two ionic interactions (O24-Arg328 at 3.50 Å, -1.9 kcal/mol; O25-Lys529 at 2.94 Å, -4.9 kcal/mol) and three hydrogen bond interactions (S14-Asn331 at 4.04 Å, -0.6 kcal/mol; O24-Gln580 at 3.18 Å, -2.0 kcal/mol; O25-Lys529 at 2.94 Å, -5.1 kcal/mol); the O25-Lys529 interactions are especially important for binding stability.Fig.15, Fig.16.

Table 8: Most Efficient Docking Results of the (NTBA) and 7JWY: VIRAL PROTEIN / 7JWY (Pose 2)

Ligand	Receptor	Interaction	Distance	E (kcal/mol)
S14 20	OD1 ASN 331 (A)	H-donor	4.04	-0.6
O24 34	NE2 GLN 580 (A)	H-acceptor	3.18	-2.0
O25 35	NZ LYS 529 (A)	H-acceptor	2.94	-5.1
O24 34	NH1 ARG 328 (A)	ionic	3.50	-1.9
O25 35	NZ LYS 529 (A)	ionic	2.94	-4.9

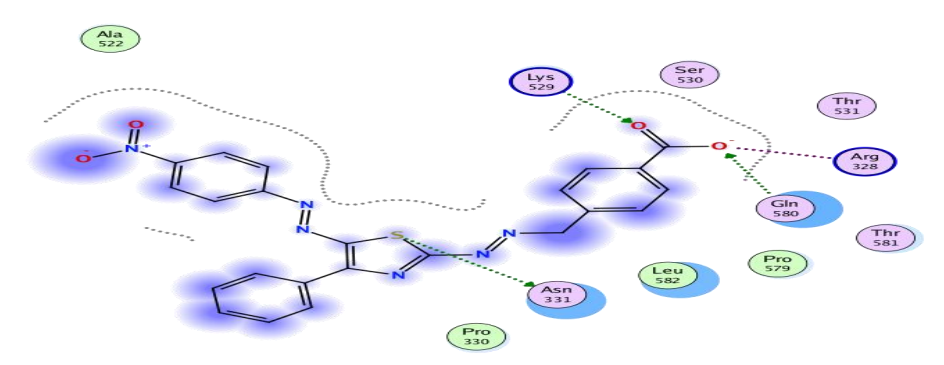


Fig. 15. 2D interaction between (NTBA) and VIRAL PROTEIN / 7JWY (Pose 2)

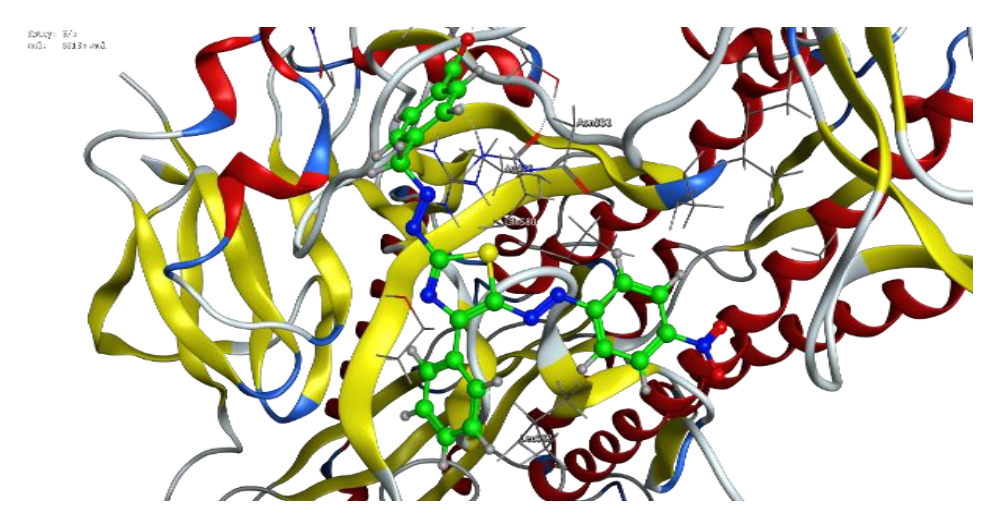


Fig. 16. 3D interaction between (NTBA) and VIRAL PROTEIN / 7JWY (Pose 2)

3.7.3 Docking Scores Comparison

The docking results table provides important energetic parameters for both binding poses:

Table 9: Comparison between the two Poses

Parameter	Pose 1	Pose 2
Final Score (S)	-5.33	-5.23
RMSD Refine	1.36	2.41
E_conf	24.07	22.35
E_place	-45.53	-59.97
E_score1	-7.97	-8.27
E_refine	-27.77	-30.15
E_score2	-5.33	-5.23

The molecular docking investigation of the ligand with the 7JWY viral protein structure indicates two energetically advantageous binding options. Despite having comparable final docking scores (S values of -5.33 and -5.23 kcal/mol, respectively), the two positions' interaction profiles and energy components differ noticeably.

With a somewhat better final score and a lower RMSD value (1.36 Å as opposed to 2.41 Å for posture 2), binding pose 1 may indicate a more stable conformation. With energy values of -5.1 and -4.9 kcal/mol, respectively, pose 2 shows stronger individual contacts, especially the hydrogen bond and ionic interactions with Lys529. These interactions play a key role in binding.

Pose 2 has a significantly more favourable placement energy (E_place) (-59.97 vs. -45.53 kcal/mol), suggesting improved initial positioning inside the binding site. Similarly, stance 2 has a lower refinement energy (E_refine) (-30.15 vs. -27.77 kcal/mol), indicating that the pose was optimized to produce a more energetically advantageous shape.

The ligand may bind to different parts of the protein, as indicated by the difference in interacting residues between the two positions. Residues Lys129, Asn125, and Val171 are interacting with stance 1, whereas Asn331, Gln580, Lys529, and Arg328 are interacting with pose 2. The mechanism of action and possible therapeutic uses may be affected by this variation in binding site preference.

Even though pose 2 final score is significantly lower than pose 1, the existence of both hydrogen bonding and ionic interactions probably adds to its refined binding energy. Pose 2's stronger ionic contacts, especially with Lys529, might offer more stability under physiological circumstances. These results offer important information for future ligand structure tuning to improve binding affinity and specificity for the viral protein target. Future research might concentrate on altering the ligand to incorporate the advantageous electrostatic interactions discovered in pose 2 while fortifying the interactions seen in pose 1.

5. Conclusion

The detailed review indicates how 4-(2-(5-(4-nitrophenyl) diazenyl)-4-phenylthiazol-2-yl) -hydrazineylidene) methyl) benzoic acid (NTBA) was effectively envisioned as a multipurpose substance that would provide clever maximum adaptability in a range of applications. Promoting the chosen synthesis approach resulted in an impressive 89% yield; consequently, the resulting material's thermal stability was verified with a melting point above 300°C, confirming its commercial-scale generation and heat resistance. The presence of a good conjugated system was demonstrated by the characterization that was done to differentiate the chemical class using IR bands and UV-Vis transitions at 528 and 264 nm,

respectively. With concentration-dependent interactions with metal ions that proceeded via diffusion-controlled processes, NTBA-modified ITO electrodes containing carboxymethyl cellulose demonstrated superior capacitance behaviour compared to the traditional platinum electrode. With IC5 o values of 29.26 mg/L (for DPPH, with 78.84% maximum scavenging) and 36.94 mg/L (for ABTS, with 63.52% maximum scavenging), strong radical scavenging properties were assessed, demonstrating significant antioxidant potential. Two binding poses with near values (-5.33 and -5.23 kcal/mol) were produced by computational analysis using the 7JWY viral protein. Pose 1 demonstrates interaction with Lys129, Asn125, and Val171 residues, while Pose 2 demonstrates stronger interaction with Lys529, Asn331, Gln580, and Arg328 residues, indicating directions of protein binding. Together, these quantitative findings establish NTBA as a previously unheard-of multipurpose platform that links items.

6. Conflicts of interest

On behalf of all authors, the corresponding author states that there is no conflict of interest.

7. Formatting of funding sources

The authors received no funding during this research

8. References and Bibliography

- [1] A.S. Radwan, M.R. Elmorsy, E. Abdel-Latif, M.M. Makhlouf, S.A. Badawy, Innovating dye-sensitized solar cells: Thiazole-based Co-sensitizers for enhanced photovoltaic performance with theoretical insights, Opt. Mater. 140 (2023) 113914
- [2] A. Dessì, M. Calamante, A. Mordini, M. Peruzzini, A. Sinicropi, R. Basosi, L. Zani, Thiazolo [5, 4-d] thiazole-based organic sensitizers with strong visible light absorption for transparent, efficient and stable dye-sensitized solar cells, RSC Adv. 5 (2015) 32657-32668.
- [3] E.M. AbouElleef, M.N. Abd El-Hady, E.A. Gomaa, A.G. Al-Harazie, Conductometric association parameters for CdBr2 in the presence and absence of Ceftazidime in water and 30% ethanol–water mixtures, J. Chem. Eng. Data 66 (2021) 878-889
- [4] M.N. Abd El-Hady, E.A. Gomaa, A.G. Al-Harazie, Cyclic voltammetry of bulk and nano CdCl2 with ceftazidime drug and some DFT calculations, J. Mol. Liq. 276 (2019) 970-985.
- [5] E.A. Gomaa, M.M. El-Defraway, S.Q. Hussien, Estimation of cyclic voltammetry data for Srcl₂, Cacl₂ and their interaction with ceftriaxone sodium salt in kNO₃ using palladium working electrode, Eur. J. Adv. Chem. Res. 1 (2020).
- [6] O.J. Fakayode, T.T. Nkambule, Cyclic voltammetric determination of calcium in water in the presence of natural organic matter (humic acid) and Cu (II) at gold electrode's surface, Food Chem. Adv. 1 (2022) 100012.
- [7] G.M. El-Sayed, S.Q. Hussein, E.A. Gomaa, M.N. Abd El-Hady, N.M. Hassan, Solvation Cyclic voltammetry Parameters for Na2WO4 in NaClO4, HCl Media and interaction with Congo Red Dye, Egypt. J. Chem. (2024).
- [8] H. Zhu, B. Hu, H. Zhang, H. Li, J. Zhou, Z. Jing, Serum Ionized Calcium as a Prognostic Biomarker in Type B Aortic Dissection After Endovascular Treatment, J. Endovasc. Ther. 32 (2025) 121-129.
- [9] E.A. Gomaa, M.A. Morsi, A.E. Negm, Y.A. Sherif, Cyclic voltammetry of bulk and nano manganese sulfate with Doxorubicin using glassy Carbon electrode, Int. J. Nano Dimens. 8 (2017) 89-96.
- [10]G.A. Mabbott, An introduction to cyclic voltammetry, J. Chem. Educ. 60 (1983) 697.
- [11]R.H. Wahba, A.Z. El-Sonbati, M.A. Diab, E.A. Gomaa, E.M. AbouElleef, Electrochemical sensing of strontium ions cyclic voltammetry and investigation of rosemary extract's effects on their behavior: Antibacterial properties of rosemary extract and molecular docking analysis for potential COVID-19 therapeutic benefits, Microchem. J. 200 (2024) 110398.
- [12]N. Tokman, The use of slurry sampling for the determination of manganese and copper in various samples by electrothermal atomic absorption spectrometry, J. Hazard. Mater. 143 (2007) 87-94.
- [13]K. Nadeau, Z. Mester, L. Yang, The direct and accurate determination of major elements Ca, K, Mg and Na in water by HR-ICPMS, Sci. Rep. 8 (2018) 17750.
- [14]R. Kowalik, The voltammetric analysis of selenium electrodeposition from H2SeO3 solution on gold electrode, Arch. Metall. Mater. 60 (2015) 57-63.
- [15] M.G. Miguel, Antioxidant activity of medicinal and aromatic plants. A review, Flavour Fragr. J. 25 (2010) 291-312.
- [16] R. Re, N. Pellegrini, A. Proteggente, A. Pannala, M. Yang, C. Rice-Evans, Antioxidant activity applying an improved ABTS radical cation decolorization assay, Free Radic. Biol. Med. 26 (1999) 1231-1237.
- [17] M.M. Hammoud, A.S. Nageeb, M.A. Morsi, E.A. Gomaa, A.A. Elmaaty, A.A. Al-Karmalawy, Design, synthesis, biological evaluation, and SAR studies of novel cyclopentaquinoline derivatives as DNA intercalators, topoisomerase II inhibitors, and apoptotic inducers, New J. Chem. 46 (2022) 11422-11436.
- [18]B.Z. Sibuh, S. Khanna, P. Taneja, P. Sarkar, N.K. Taneja, Molecular docking, synthesis and anticancer activity of thiosemicarbazone derivatives against MCF-7 human breast cancer cell line, Life Sci. 273 (2021) 119305.
- [19]S. Bondock, O. Albormani, A.M. Fouda, Facile Synthesis and Anticancer Evaluation of Novel 1-(Thiazol-2-yl)-3-(thiazol-5-yl)-5-(thiophen-2-yl) Pyrazolines, Russ. J. Gen. Chem. 92 (2022) 1098-1108.
- [20]K. Liu, H. Lu, L. Hou, Z. Qi, C. Teixeira, F. Barbault, L. Xie, Design, synthesis, and biological evaluation of N-carboxyphenylpyrrole derivatives as potent HIV fusion inhibitors targeting gp41, J. Med. Chem. 51 (2008) 7843-7854.
- [21]S.A. Badawy, E. Abdel-Latif, M.A. Assiri, T.E. Ali, M.R. Elmorsy, Hydrazonothiazole dyes for enhanced dye-sensitized solar cells in greenhouse applications: Achieving high power conversion efficiency and long-term stability, Dyes Pigm. 217 (2023) 111447.

- [22] M.M. El-Kerdawy, R.I. El-Bagary, E.F. Elkady, A.A. Othman, Development and validation of a stability-indicating RP-LC method for the simultaneous determination of otilonium bromide and its expected degradation product in bulk drug and pharmaceutical preparation, Eur. J. Chem. 7 (2016) 97-101.
- [23]E.A. Gomaa, A.Z. El-Sonbati, M.A. Diab, M.S. El-Ghareib, H.M. Salama, Cyclic voltammetry, kinetics, thermodynamic and molecular docking parameters for the interaction of nickel chloride with diphenylthiocarbazone, Open Acad. J. Adv. Sci. Technol. 4 (2020) 30-44.
- [24] M.A.F. Othman, A.A. Othman, H.M. Zuki, Dithizone modified silver electrode for the determination of metal ions in aqueous solution, Malays. J. Anal. Sci. 20 (2016) 197-204.
- [25]S. Birghila, M.M. Bratu, C. Prajitura, F.N. Roncea, T. Negreanu-Pirjol, Spectrophotometric method for the determination of total proteins in egg white samples, Rev. Chim. 66 (2015) 378-381.
- [26]B.H. Durmishi, M. Ismaili, A. Shabani, S. Jusufi, X. Fejzuli, M. Kostovska, S. Abduli, The physical, physical-chemical and chemical parameters determination of river water Shkumbini (Pena)(part A), Ohrid, Republic of Macedonia 27 (2008) 1-11
- [27] A.A. Olajire, F.E. Imeokparia, Water quality assessment of Osun River: studies on inorganic nutrients, Environ. Monit. Assess. 69 (2001) 17-28.
- [28]R. Gruden, A. Buchholz, O. Kanoun, Electrochemical analysis of water and suds by impedance spectroscopy and cyclic voltammetry, J. Sens. Sens. Syst. 3 (2014) 133-140.
- [29]A.F. El-Baz, H.M. Abbas, Isolation and identification of an endophytic fungus from ficus elastica decora and investigation of the antioxidant and antifungal bioactivities of its fermentation extract, Menoufia J. Agric. Biotechnol. 2 (2017) 81-85.
- [30] A. Mohamed, S. Yousef, W.S. Nasser, T.A. Osman, A. Knebel, E.P.V. Sánchez, T. Hashem, Rapid photocatalytic degradation of phenol from water using composite nanofibers under UV, Environ. Sci. Eur. 32 (2020) 1-8.
- [31]D.A. El-Kot, E.A. Gomaa, A.M.H. El-askalany, R.R. Zaky, M.N. Abd El-Hady, Design of a novel-NOON-tetradentate Schiff-base scaffold supported by α-tetralone and benzothiazole moieties with its Cu2+, Co2+, and Cd2+ chelates, J. Mol. Struct. 1278 (2023) 134901.
- [32]H. Ye, R.M. Crooks, Electrocatalytic O2 reduction at glassy carbon electrodes modified with dendrimer-encapsulated Pt nanoparticles, J. Am. Chem. Soc. 127 (2005) 4930-4934.
- [33] J.M. Almeida, R.M. Dornellas, S. Yotsumoto-Neto, M. Ghisi, J.G. Furtado, E.P. Marques, A.L. Marques, A simple electro analytical procedure for the determination of calcium in biodiesel, Fuel 115 (2014) 658-665.
- [34]E.A. Gomaa, M.A. Tahoon, A. Negm, Aqueous micro-solvation of Li+ ions: Thermodynamics and energetic studies of Li+-(H2O) n (n= 1-6) structures, J. Mol. Liq. 241 (2017) 595-602.
- [35]E.A. Gomaa, R.R. Zaky, A. Shokr, Estimated the physical parameters of lanthanum chloride in water-N, N-dimethyl formamide mixtures using different techniques, J. Mol. Liq. 242 (2017) 913-918.
- [36]E.A. Gomaa, M.H. Mahmoud, M.G. Mousa, E.M. El-Dahshan, Cyclic Voltammetry for the interaction between Bimthus Nitrate and Methyl Red in Potassium Nitrate Solutions, Chem. Methodol. 3 (2018) 1-144.
- [37] M. Fathi, E.A. Gomaa, S.E. Salem, H.M. Killa, A.A. Gouda, A.H. Farouk, Parameters for the conductometric association for lump and nano CoSO4. 7H2O in the presence and absence of fuchsin acid in water at different temperature, Bull. Chem. Soc. Ethiop. 37 (2023) 789-804.
- [38] J. Nakanishi, I. Kuramoto, J. Baba, K. Ogawa, Y. Yoshikawa, H. Ishiguro, Continuous hospitality with social robots at a hotel, SN Appl. Sci. 2 (2020) 1-13.
- [39]E.M. AbouElleef, M.N. Abd El-Hady, E.A. Gomaa, A.G. Al-Harazie, Conductometric association parameters for CdBr2 in the presence and absence of Ceftazidime in water and 30% ethanol—water mixtures, J. Chem. Eng. Data 66 (2021) 878-889.
- [40]D. Kayali, N.A. Shama, S. Asir, K. Dimililer, Machine learning-based models for the qualitative classification of potassium ferrocyanide using electrochemical methods, J. Supercomput. 79 (2023) 12472-12491.
- [41]F.J. Rossotti, H. Rossotti, The determination of stability constants, and other equilibrium constants in solution, (No Title) (1961).
- [42] M.D. Murray, B. Loos, W. Tu, G.J. Eckert, X.H. Zhou, W.M. Tierney, Effects of computer-based prescribing on pharmacist work patterns, J. Am. Med. Inform. Assoc. 5 (1998) 546-553.
- [43] A.A. Sharfalddin, A.H. Emwas, M. Jaremko, M.A. Hussien, Synthesis and theoretical calculations of metal-antibiotic chelation with thiamphenicol: in vitro DNA and HSA binding, molecular docking, and cytotoxicity studies, New J. Chem. 45 (2021) 9598-9613.
- [44]B.A. Babgi, N.A. Alzaidi, J.H. Alsayari, A.H.M. Emwas, M. Jaremko, M.H. Abdellattif, M.A. Hussien, Synthesis, HSA-Binding and Anticancer Properties of [Cu2 (μ-dppm) 2 (N[^] N) 2] 2+, J. Inorg. Organomet. Polym. Mater. 32 (2022) 4005-4013.
- [45] N. Daud, S.M.M. Nor, N.A. Yusof, Electrochemical characteristic of biotinyl somatostatin-14/Nafion modified gold electrode in development of sensor for determination of Hg (II), Int. J. Electrochem. Sci. 8 (2013) 10086-10099.
- [46]Q. Yin, Z. Xu, T. Lian, D.G. Musaev, C.L. Hill, Y.V. Geletii, Tafel slope analyses for homogeneous catalytic reactions, Catalysts 11 (2021) 87.
- [47]T. Shinagawa, A.T. Garcia-Esparza, K. Takanabe, Insight on Tafel slopes from a microkinetic analysis of aqueous electrocatalysis for energy conversion, Sci. Rep. 5 (2015) 13801.